Available online at www.sciencedirect.com
ScienceDirect
Applied Surface Science 253 (2006) 833–840
applied surface science
www.elsevier.com/locate/apsusc

Atomistic modeling of dislocation activity in nanoindented GaAs

Sheng-Rui Jian [a], Te-Hua Fang [b,*], Der-San Chuu [a], Liang-Wen Ji [c]

[a] Department of Electrophysics, National Chiao Tung University, Hsinchu 300, Taiwan
[b] Institute of Mechanical and Electromechanical Engineering, National Formosa University, Yunlin 632, Taiwan
[c] Department of Electro-Optics Engineering, National Formosa University, Yunlin 632, Taiwan

Received 4 October 2005; received in revised form 11 January 2006; accepted 11 January 2006
Available online 13 February 2006

Abstract

The mechanical behavior of GaAs was investigated by nanoindentation with the aid of molecular dynamics (MD) analysis based on the Tersoff potential. Particular attention was devoted to the evolution characterization of dislocation activity during deformation. The transition from elastic-to-plastic deformation behavior was clearly observed as a sudden displacement excursion occurring during the load–displacement curves of larger loads (single pop-in), faster impact velocity and higher temperature (multiple pop-ins). Even for an ultra-small penetration depth (<3 nm), the MD simulation shows that GaAs deforms plastically and a good description is given in the results. The plastic deformation occurs due to the anticipated change in the twinning and/or dislocation motion. Dislocation nucleations occurred inside the material near the top of the surface and generated loops in the {1 1 1} slip planes. The MD analysis of the deformation behavior shows an agreement with that of previous atomic force microscopy (AFM) and transmission electron microscopy (TEM) experiments.

PACS: 02.70.Ns; 62.20.-x; 62.25.+g

Keywords: Molecular dynamics simulations; Tersoff potential; GaAs; Nanoindentation

1. Introduction

Recent developments in science and technology have advanced the capability to fabricate and control structures on the nanometer-scale. In designing nanodevices, mechanical properties are essential since most mechanical properties exhibit a size-dependent effect. Many potential applications for these nanostructures are not really practical because their mechanical properties have not been established. Therefore, an accurate measurement of the mechanical characterizations of nanomaterials, such as the hardness, dislocation motion and Young's modulus, is required to be able to use them as structural/functional elements in devices. In this field, an excellent method to measure mechanical properties in small regions of a material is that of nanoindentation. Nanometer-range indentation depth can be utilized to probe materials whose thickness is on a nanoscale. It has been widely used to characterize structural and mechanical properties of materials and thin films [1–6].

In spite of these experimental observations, the mechanisms on an atomic-scale are not well understood. For atomic length scales, the continuum models of deformation do not perform well and atomistic methods need to be considered to investigate the deformation behavior on a nanometer-scale. First-principle simulations are too expensive, limiting the maximum indentation depth to a few angstroms only [7], which are quite far away from the actual experimental depths. The quasicontinuum method [8] is able to simulate surface indentation up to a depth of several tens of nanometers, but it misses the atomistic aspects such as the defect formation, local transition elastic–plastic behavior and phase transformations.

Atomistic simulations based on molecular dynamics (MD) can be used to obtain quality interatomic potentials and theoretical studies to analyze the experimental data and extract reliable information. By virtue of it is high temporal and spatial resolutions, MD simulations offer novel insight into the atomic-scale process and understanding of their mechanisms. Landman et al. [9] found two different phenomena took place in their Ni tip/Au substrate model during the indentation and retraction processes. One is the jump-to-contact caused by mechanical instabilities in the nanoindentation phase. The other is the

* Corresponding author. Tel.: +886 5 631 5395; fax: +886 5 631 5394.
E-mail address: fang.tehua@msa.hinet.net (T.-H. Fang).

0169-4332/$ – see front matter © 2006 Elsevier B.V. All rights reserved.
doi:10.1016/j.apsusc.2006.01.022

connective neck formed at the interface between the tip and the substrate because of a strong attractive bonding between the metals. In addition to these, Li et al. [10] and Vlient et al. [11] pointed out that the location and critical stress of homogeneous nucleation could be predicted by the ''Λ-criterion''. This criterion also provides some clues as to what kinds of defects may result after the instability. If the unstable elastic wave is longitudinal (sound wave), then a microcrack is likely to be nucleated. If the unstable elastic wave is transversed (shear wave), then a dislocation loop or twinning embryo may be nucleated. Limited by computation power, most of the systems studied in atomic simulations are not large enough to produce accurate results. Recently, Vashishta and co-authors [12,13] reported that significant plastic deformation and pressure-induced amorphization of α-Si_3N_4 occurred under a Vickers indenter using MD simulations.

Scanning electron microscopy (SEM), atomic force microscopy (AFM), scanning tunneling microscopy (STM) and transmission electron microscopy (TEM) techniques, used in nanoindentation experiments, are able to detect dislocations; nevertheless, it is difficult to resolve the atomistic structures and dynamics of dislocations in detail [14]. Herein, it is important to begin a systematic study to investigate qualitatively, various factors that dominate nanoindentation behaviors. To our knowledge no work on the influence of load, impact velocity and temperature on nanoindentation-induced deformation behaviors of GaAs has been accomplished through MD analysis. The results are of particular significance because the physical mechanism, which operates during the deformation of a contact, has a direct effect on the mechanical responses of the material's surface under indentation. The goals of this study are threefold: (1) to determine the atomic-scale mechanisms of nanoindentation, (2) to examine the dislocation structural changes of GaAs in the course of the nanoindentation process, and (3) to compare the computational mechanical properties of GaAs to the experimental results.

2. Molecular dynamics

In MD simulations the physical system is described by sets of N atomic positions $\{\vec{r}_i | i = 1, \ldots, N\}$ and velocities $\{\vec{r}_i | i = 1, \ldots, N\}$. Time is dissected into discrete intervals and can be used to numerically solve Newton's equation of motion with the potential $V(\{\vec{r}_i\})$

$$m_i \frac{\mathrm{d}^2 \vec{r}_i(t)}{\mathrm{d}t^2} = -\frac{\partial V}{\partial \vec{r}_i} \tag{1}$$

MD simulations were carried out based on the Tersoff potential [15] to investigate the nanoindentation-induced plastic deformation behaviors of GaAs using a diamond tip, which involved both two-body and three-body terms

$$V = \frac{1}{2}\sum_{i \neq j} u_{ij} \quad \text{where} \quad u_{ij} = f_{\mathrm{C}}(r_{ij}) | f_{\mathrm{R}}(r_{ij}) + b_{ij} f_{\mathrm{A}}(r_{ij}) | \tag{2}$$

Here i and j are labels for the atoms. The term f_{R} denotes a repulsive pair potential due to the overlapping electrons, while f_{A} denotes an attractive pair potential associated with bonding. The function f_{C} is merely a smooth cutoff function to limit the potential range. The coefficient b_{ij} (the bond order) corresponds to a many-body interaction of the form

$$b_{ij} = \chi_{ij}(1 + \beta_i^{n_i} \zeta_{ij}^{n_i})^{-1/2n_i}, \tag{3}$$

$$\zeta_{ij} = \sum_{k \neq i,j} f_{\mathrm{C}}(r_{ik}) g(\theta_{ijk}) \quad \text{where}$$
$$g(\theta_{ijk}) = 1 + \frac{c_i^2}{d_i^2} - \frac{c_i^2}{d_i^2 + (h_i - \cos\theta_{ijk})^2} \tag{4}$$

and the constants χ_{ij} , β_i, n_i, c_i, d_i and h_i depend on the atomic species [15] and θ_{ijk} is the bond angle between the ij and ik bonds. In addition, the parameters between two different materials were calculated using the mixing rules. Other parameters values can be found in Ref. [16].

In this simulation the GaAs substrate was modeled as a finite slab (30 × 30 × 10 layers) containing 72,000 atoms placed in a zinc-blende (ZB) structure with a lattice constant of 0.565 nm, corresponding to the room temperature lattice constant for GaAs. The diamond indenter tip is a three-sided pyramidal Berkovich shape containing 5900 atoms with a lattice constant of 0.357 nm and a tip radius of 2 nm. The reason for the lattice constants using three decimal accuracy values is kept the precision of the simulation in the initial condition. It is important to point out that a rigid diamond indenter is both harder (plastically) and stiffer (elastically). Thus, in all simulations the indenter is assumed to be rigid. This is a reasonable approximation since a diamond tip is significantly harder than GaAs. The tip was placed above the substrate, so at the beginning there is no interaction between the tip and substrate. Starting at 1 nm above the sample, the pyramidal indenter is placed into and then removed from the sample at the same speed.

The equation of motion was integrated using the Verlet algorithm [17] with a time step of 1 fs, and the atomic configurations were recorded every 5000 time steps. At each temperature the sample is first equilibrated for a period of 50 ps, which was much longer than the time needed for the system to reach equilibrium. Periodic boundary conditions [17] were used in the transverse (x- and y-directions) while the free surface was allowed to relax in the z-direction. The bottom five layers of atoms were fixed in space [18]. In addition, thermostat atoms were in the next two upper layers as well as the sides of the GaAs and their temperature was kept fixed in order to dissipate any heat produced during the nanoindentation process. The purpose of the thermostat atom layers was to absorb the heat and conduct outwards the control volume [19]. The kinetic energy is in proportion to the temperature of the atom, so the temperature of these layers should not be changed.

3. Results and discussion

3.1. Nanoindentation response

The simulated load–displacement curve for GaAs under an indentation velocity of 30 m/s at 300 K is plotted in

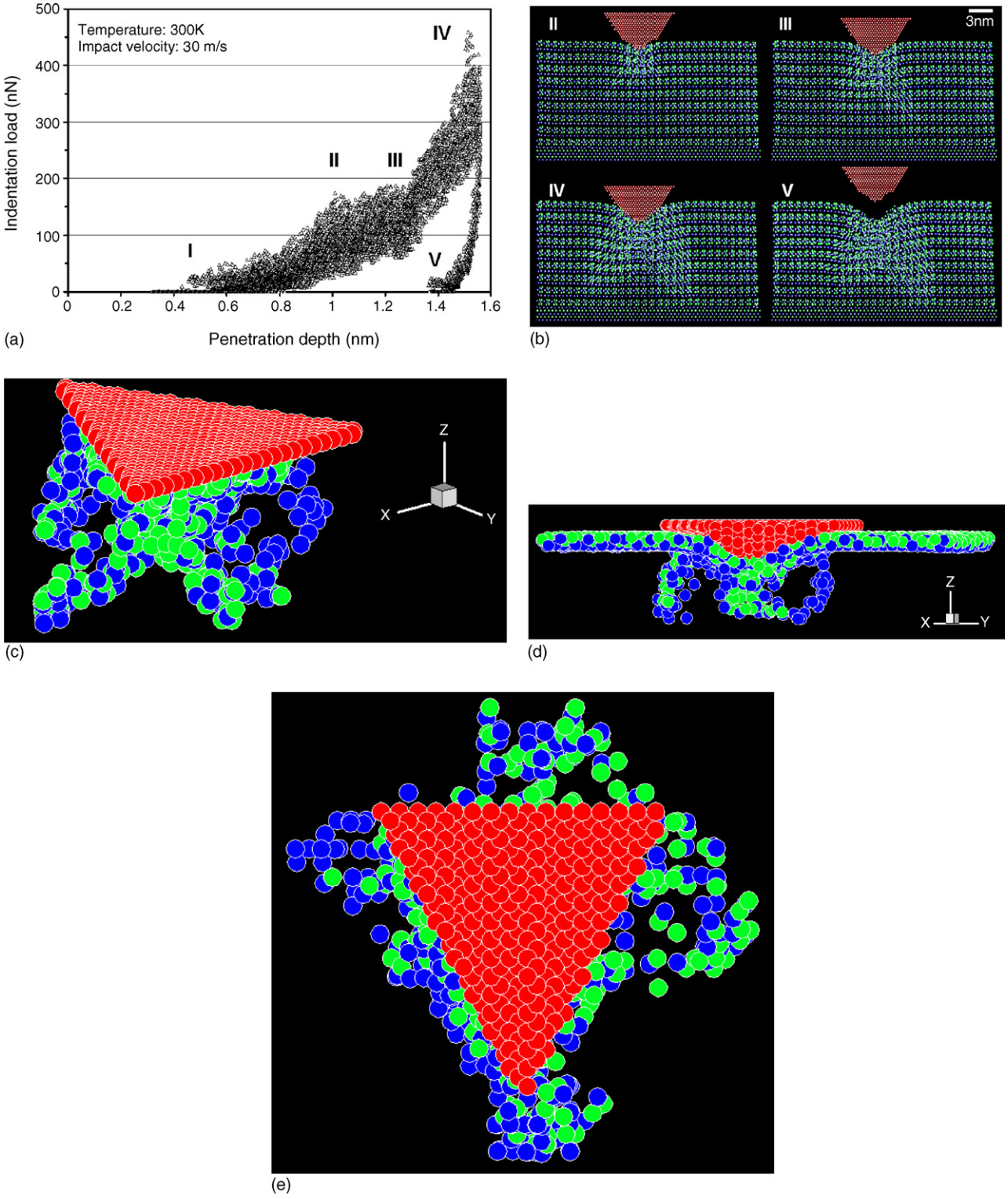

Fig. 1. (a) Load–displacement data for GaAs obtained during nanoindentation with a Berkovich indenter showing pop-in behavior during loading, (b) the cross-sectional view of the (0 1 0) plane corresponds to II–V steps, (c) 3D MD simulation views of the dissociated dislocation loops, (d) the cross-sectional view of dislocation loops surrounded the indenter tip and rotating 30° along the [1 1 1] plane (corresponding to the IV step), and (e) top view of the MD simulation surface showing the dislocation loops formed on and under the {1 1 1} plane. Red, green and blue represent the C, Ga and As atoms, respectively. (For interpretation of the references to color in this figure legend, the reader is referred to the web version of the article.)

Fig. 1(a). A pop-in event was observable in the course of the plastic deformation: the initial yielding was related to the onset of plasticity, since the deformation behavior prior to yield excursion is elastic (please see the portion from I to II). The elastic response continued to a penetration depth of about 1 nm. As might be expected, the response was an elastic behavior with a slight change to the slope due to the trapping of new atoms.

The initial dislocation nucleation beneath the tip is observed at step II and the well-known embryonic dislocations and coalesce phenomena immediately developed from the sites of the homogeneous nucleation, as can be seen in the prospective close-up view of Fig. 1(b). The initial plastic response of GaAs under indentation is deformed by twinning and/or dislocation propagation (slip) in which the dislocation nucleation processes were oriented along the slip planes located at ±30° from the vertical. When increasing the penetration depth, the slip (twinning) system occurred predominantly on the {1 1 1} planes that terminated at the (0 0 1) surface.

Upon retraction of the indenter tip, the indenter is separated from the crystal surface at a penetration depth of 1.38 nm. The deformed region underwent incomplete elastic recovery which indicates that the plastic deformation rearrangement was irreversible and had resulted in a permanent plastic deformation. At the end, upon full removal of the load, several dislocations remained on the GaAs surface. These dislocations were mainly those that had been moved laterally and closer to the surface of the indented material (please see the portion at V).

These dislocations are generated/entangled beneath the indenter, as schematically shown in Fig. 1(c)–(e). The dislocation nucleation during displacement-controlled nanoindentation occurred near the surface as expanding glide loops at the {1 1 1}⟨1 1 0⟩-slip systems. The nucleation of interstitial dislocation loops by a punching mechanism just beneath the pyramidal indenter was the condition that further propagated the dissociated dislocations. The expanding glide loops intersected the surface were shown to originate from loops of interstitial character emitted along the ⟨1 1 0⟩ direction. Fig. 1(d) shows the generation of embryonic dislocation loops giving rise to the pop-in event. The generation of the loops can be understood as a homogeneous dislocation nucleation. Fig. 1(e) illustrates the dislocation loops that propagate in the in-plane direction and were terminated by edge dislocations on the surface. There is clear reflection symmetry along the [1 1 0] direction. The partial dislocation emitted glide loops, either along or below the surface were of great importance because they propagate the permanent deformation away from the vicinity of the indenter tip.

As shown in Fig. 2(a), the same loading pattern is seen for indents on a GaAs surface at a maximum load of 1400 μN with the pop-in event occurring at a load of about 200 μN, which is in line with Fig. 1(a). The larger indentation load causes the deeper twinning bands to propagate to where it appears to interact and intersect, as shown in Fig. 2(b). In addition, the dislocation structure extends over a wider region and contains denser dislocation loops which bonded into a stacking shape larger then the size of the contact area. As mentioned above, the nanoindentation-induced deformation of GaAs was primarily dominated by twinning in alignment along the {1 1 1} plane, which was the glide plane in the zinc-blende crystal.

Fig. 3(a) shows the simulated load–displacement curve for GaAs under the indentation velocity of 30 m/s at 700 K.

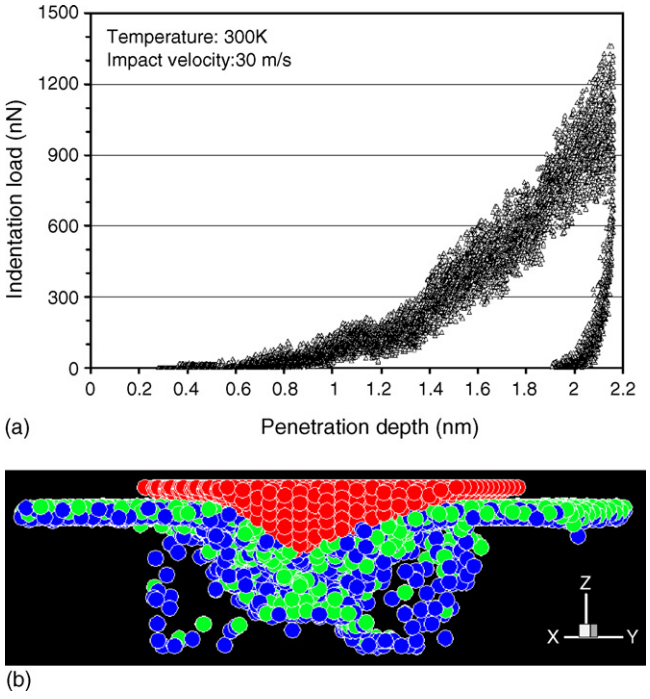

Fig. 2. (a) The load vs. displacement curve at a penetration depth of 2 nm and (b) illustrates the cross-sectional view of dislocation loops surrounded the indenter tip and rotating 30° along the [1 1 1] plane at peak load.

Multiple pop-ins were clearly observed during the loading process. After the initial yielding point the load increased continuously and elastically and then the material yielded again, repeating this process until the maximum load or the

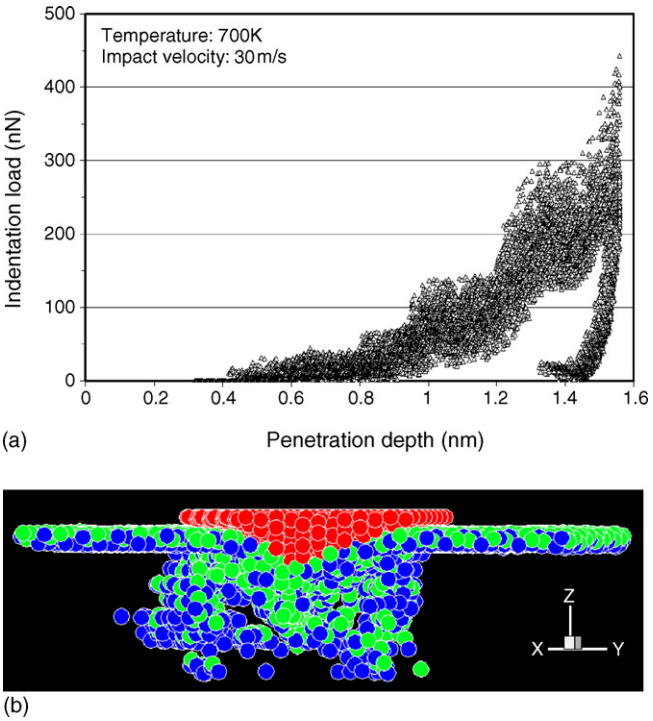

Fig. 3. (a) The load vs. displacement curve at a temperature of 700 K and (b) illustrates the cross-sectional view of dislocation loops surrounded the indenter tip and rotating 30° along the [1 1 1] plane at peak load.

maximum penetration depth was attained. Two major trends observed in MD simulations were evident in the curves presented in Figs. 1(a) and 3(a). First of all, indentation on GaAs at 300 and 700 K revealed that the elastic-to-plastic response occurred progressively at lower stress levels and as the temperature was increased; second, the number of pop-ins increased noticeably with an increase in the temperature. Fig. 3(b) illustrates the dislocations underneath the indenter tip at the indentation's peak load. With the dislocations nucleating around the periphery of the indented area, it seems reasonable that more complicated entanglements would be possible at higher temperatures. These results are expectation for thermally activated deformation processes such as the dislocations nucleation and/or entanglements.

Comparing Figs. 1(a)–4(a), it can be seen that multiple pop-ins occurred on the simulated load–displacement curve at an impact velocity of 120 m/s and a temperature of 300 K. Fig. 4(b) displays the computed dislocation structures that surround the indenter tip. Owing to the faster impact velocity rapid multiplication of dislocations occurred around the indenter tip at the instant it came in contact with the material's surface. The main difference is that the generation of dislocations on the surface in the contact area had a lower load when the first pop-in was observed and, at faster impact velocities showed a far weaker twin structure.

In exploring the dislocation reactions, which occurred in the course of nanoindentation of a ZB structure, it is convenient to adopt the Thompson tetrahedron notation [20]. As shown in Fig. 5, it can be seen that the four different sets of {1 1 1} planes are parallel to the four faces of a regular tetrahedron, whose edges are parallel to slip ⟨1 1 0⟩-direction. In the course of

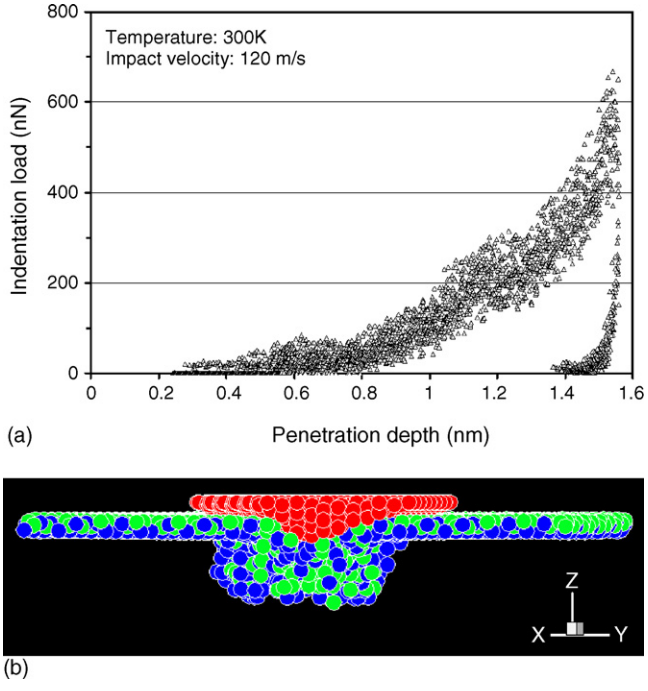

Fig. 4. (a) The load vs. displacement curve with an impact velocity of 120 m/s and (b) illustrates the cross-sectional view of dislocation loops surrounded the indenter tip and rotating 30° along the [1 1 1] plane at peak load.

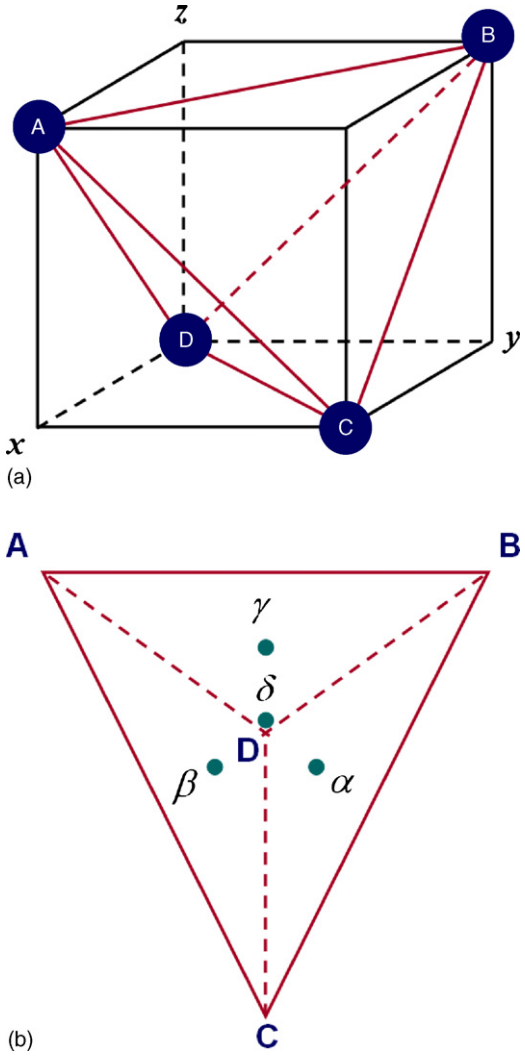

Fig. 5. (a) The tetrahedron formed by the joining of the four nearest adjacent sites *ABCD* in an fcc crystal and (b) the Thompson's tetrahedron, with the midpoints of the four planes being labeled as α, β, γ and δ.

nanoindentation, the indentation-induced dislocation nucleations and glides were along segment *BD* in the *ABD* and *BCD* planes. The ideal dislocation on the *ABD* and *BCD* planes would split the {1 1 1} plane with the reactions.

$$BD \rightarrow B\gamma + \gamma D; \quad BD \rightarrow B\alpha + \alpha D \tag{5}$$

This is in agreement with Ref. [20], therefore reasonable results were obtained in this study's MD analysis. A higher hardness is measured at a higher impact velocity. This is due to the higher impact velocity causes a larger shear strain rate on the localized distortion in the lattice near the indented area. The screw dislocations lie on {1 1 1} planes with Burger vector $\mathbf{b} = a/6\ [2\bar{1}\bar{1}]$ and are easier to be dissociated into 30° partials separated by a stacking fault in GaAs. The glide leads to the formation of a high-energy stacking fault. The two chemical species present in GaAs lead to two types of partial dislocations: the Ga atmos can be, given γ dislocations, or As ones leading to α dislocations. A screw dislocation dissociates into two 30° partials: one of Ga-type

and the other of As-type. The 60° dislocation dissociates into a 30° and a 90° partial of the same type. The lowest energy partials are of the glide type.

During the entire dislocation evolution, some notable steps were analyzed in detail, focusing on the dislocation nucleations, dislocation loops and specific evolution patterns while indenting the GaAs surface. It is clearly observed that the slip and/or twinning dislocation nucleations occurred on adjacent {1 1 1} plane and where emitted from the corners of the indenter during the nanoindentation of GaAs. Here, MD simulations are in strong agreement with recent AFM and cross-sectional transmission electron microscopy studies [21–23]. These studies showed that the slip traces along the edges of the indented region on a GaAs surface [21] and the dislocation glide and motion along the {1 1 1} plane. Furthermore, the twinning behavior at room temperature is primarily caused by the loading conditions. Even at high temperatures, it was observed that the indentation-produced dislocations beneath the indenter with mechanical deformation predominantly occurring by the dislocation's movement [22]. In addition, Mann and Pethica [23] pointed out that the high-velocity impacts could cause multiple pop-ins in the course of the plastic deformation which also supports the MD observations in this study. With the weak-beam technique of electron microscopy, Patriarche and Le Bourhis [24] observed the dislocation density was very high in the plastic zones in GaAs and only the edges of the plastic zone showed individual dislocation lines. Taylor et al. [25] proved implications regarding the indent induced dislocation strain fields of GaAs. Plastically deformed solely by dislocation nucleation and propagation for loads less than 400 μN and indentation depths less than 50 nm. Also their TEM images showed that the dislocation density and plastic zone size introduced into the material. In closing, it is propose that MD simulations provide quantitative insights into the mechanical deformation of nanoindentation processes and when analyzed in a statistical framework it could help to in terpret complex mechanical behaviors.

3.2. Comparison of the experiments and MD simulations

The goal of this experiment was to verify the results obtained by MD analysis. Several difficulties were encountered when comparing the nanoindentation experiments to MD simulation, such as, the dimensional scale of nanometers to the atomic-scale and the temporal scale of seconds to picoseconds. Despite the differences in the scales inherent in the nanoindentation experiments and MD simulations, there was consistent agreement between the experimental results and the MD simulation in regards to the plastic behaviors in the local region.

3.2.1. Experimental details

A Triboscope nanoindentation system (Hysitron Incorporation) was used to perform the nanoindentation tests on a single-crystal GaAs (1 0 0). The root-mean-square roughness and average surface roughness of the GaAs surface were less than 0.2 and 0.3 nm, respectively.

The hardness and elastic modulus were calculated from the load–displacement data obtained from nanoindentation using a three-sided pyramidal diamond Berkovich indenter tip with a tip radius of 50 nm. The nanoindenter monitored and recorded the load and displacement of the indenter during indentation with a force resolution of about 1 μN and had a displacement resolution of 0.2 nm. A typical indentation experiment consisted of four sequential steps: approaching the surface, loading to the peak load, holding the indenter at the peak load for 5 s and then finally unloading completely. The hold step was included to avoid the influence of creep during unloading. All nanoindentation tests were performed when the thermal drift was dropped down to 0.01 nm/s. The thermal drift effect was avoided by utilizing the hold step during each test.

Nanoindentation hardness [26] was defined as the indentation load divided by the projected contact area of the indentation, meaning that the mean pressure that a piece of material will support under a load. From the load–displacement curve, hardness was obtained at the peak load P_{max} as

$$H = \frac{P_{max}}{A_c} \tag{6}$$

where A_c is the projected contact area.

The elastic modulus was calculated using the Oliver-Pharr data analysis procedure [26], beginning by fitting the unloading curve to the power–law relationship. The unloading stiffness S was obtained from the slope of the initial portion of the unloading curve. The geometry indentation relationship among the contact stiffness, contact area and elastic modulus was derived as follows:

$$S = 2\beta E_r \sqrt{\frac{A_c}{\pi}} \tag{7}$$

where β is a constant value of 1.034 for a Berkovich indenter [26], and E_r is the reduced elastic modulus, which supports that elastic deformation occurs in both the specimen and the indenter. E_r is given by

$$\frac{1}{E_r} = \frac{1-\nu_i^2}{E_i} + \frac{1-\nu_m^2}{E_m} \tag{8}$$

where E_i and ν_i are the Young's modulus and the Poisson's ratio of the indenter, respectively. E_m and ν_m are the respective parameters of the materials being tested. For a diamond indenter, E_i = 1141 GPa and ν_i = 0.07[24]. Here, the value of ν_m for GaAs was assumed to be 0.3 in all calculations.

To calculate the hardness, contact stiffness and elastic modulus using Eqs. (6)–(8), the projected contact area A_c was determined from the load–displacement curve. It was assumed that the indenter used in practical nanoindentation testing was not ideally shaped. Thus, the tip geometry calibration or the area function calibration was needed. A series of indentations was made on fused silica at the depths of interest. The computed area was plotted as a function of the contact

depth to fit the A_c versus h_c and used a fifth order curve consisting of terms relating to the deviation from a perfect tip geometry, as follows:

$$A_c = 24.56h_c^2 + 1.42 \times 10^4 h_c - 4.62 \times 10^5 h_c^{1/2} + 9.72 \times 10^5 h_c^{1/4} + 3.17 \times 10 h_c^{1/8} \quad (9)$$

The parameters of Eq. (9) were then inputted into the data analysis section of the Hysitron Triboscope nanoindenter for use on further indentations made at depths in the recorded calibration range. The analysis software of the Triboscope system had the capability to automatically calculate the nanomechanical properties and then correct the tip's calibration.

The contact depth was estimated from the load–displacement data using

$$h_c = h_{max} - \varepsilon \frac{P_{max}}{S} \quad (10)$$

where ε is a constant that depends on the indenter geometry ($\varepsilon = 0.75$ for a Berkovich indenter) and h_{max} is the displacement at the peak load [26].

3.2.2. Plasticity in GaAs under nanoindentation

At the onset of the irreversible deformation, the interstitial dislocation loops nucleated. This phenomenon was probably related to the fact that the plastic deformation was dominated by pop-in events [14]. When the loading was larger than the yielding point and permanent plastic deformation occurred, possibly one mechanism could account for this phenomenon and that is the activation of the dislocation sources. These applied stresses increased until a new dislocation source was formed, which resulted in a larger release of dislocations generated throughout the entire plastic zone around the nanoindentation. Once the entire plastic zone had developed, there were many dislocation sources and there was no discontinuity in the loading curve.

The above results made it clear that the (first) pop-in corresponded to the elastic-to-plastic transition, that is, it was the onset of plasticity in GaAs. Therefore, the maximum shear stress within the GaAs represents its shear strength when this (first) pop-in occurred. It has been identified that the processes responsible for this pop-in were associated with the dislocation nucleations. The first critical load (P_c), the maximum elastic shear stress (τ_{max}) underneath an indenter are given by the relationship [27]

$$\tau_{max} = 0.31 \left(\frac{6P_c E_r^2}{\pi^3 R^2} \right)^{1/3} \quad (11)$$

In this study Table 1 summarizes the hardness, Young's modulus and the maximum shear stress at the first pop-in. The differences between the experimental and the simulated results were attributed to a number of factors, including experimental scatter, surface roughness and the presence of defects in the GaAs material used in the experiment. In addition, the experimental indentation depth was larger than that of the MD simulation. The simulation was affected by the surface response. Furthermore, the reconstruction effect on the surface may have also caused the unloading curve to be steeper and thus yielding a higher estimated value for Young's modulus. More specifically, the defect's influence on the deformation mechanism of the material was different for different size scales. The calculated hardness being larger than the experimental hardness may be ascribed to the hardness experimental data not having a constant value. When the indentation depth was reduced, the indentation size effect would cause the hardness to increase.

Table 1
Mechanical properties of GaAs investigated in this study

MD simulations	Maximum shear stress at first pop-in, τ_{max}	Young's modulus, E_m	Hardness, H
Loads[a]	18.6 ± 1.2	184.1 ± 8.3	8.6 ± 0.8
Impact velocities[b]	13.6 ± 3.7	150.3 ± 42.1	10.3 ± 0.5
Temperatures[c]	11.2 ± 6.1	148.2 ± 27.6	7.6 ± 1.8
Nanoindentation tests			
Loads	21.2 ± 0.4[d]	104.6 ± 8.4[d]	10.2 ± 0.6[d]
	~4.5[27]	~97[27]	~7.5[27]
Impact velocities	18.2 ± 0.7[e]	100.2 ± 0.7[e]	9.8 ± 0.2[e]
Temperatures	–	–	5.0 ± 2.5[22]
			4.3 ± 3.2[22]

[a] P_c: 175–200 μN with impact velocity of 30 m/s at 300 K.
[b] P_c: 100–175 μN with impact velocity of 30–120 m/s at 300 K.
[c] P_c: 50–175 μN with impact velocity of 30 m/s at 300–700 K.
[d] P_c: 480–500 μN with loading-rate of 10 μN/s at RT.
[e] P_c: 220–350 μN with loading-rate of 250–2000 μN/s at RT.

4. Conclusions

The nanoindentation-induced dependence of the twinning and dislocation nucleation behaviors in GaAs was investigated by MD simulations. In the plastic range of the load–displacement curve, the pop-in(s) effect was observed in all MD simulations and was associated with the dislocation nucleation activity beneath the indenter tip. During the process of indentation the dislocation structure comprised of dislocation glide loops on the adjacent {1 1 1} slip plane. These dissociated loops, which intersected the surface, were shown to originate from the interstitial character loops emitted along the ⟨1 1 0⟩ direction. Based on the local strain diagnostic, the mechanical deformation processes were closely related to the coupling of the dislocation-mediated; plasticity, nucleation and propagation of slip (twinning). The deformation twinning systems observed, occurred at lower temperatures and/or slower impact velocity during nanoindentation. In addition, the effect that temperature had on the generation of dislocations was an important aspect to consider for realistic simulations of nanoindentations.

Acknowledgements

This work was partially supported by the National Science Council of Taiwan, under Grant Nos. NSC 94-2212-E-150-045

and NSC 94-2212-E-150-046. The authors like to thank Mr. Yen-Hung Lin for his technical support.

References

[1] R. Navamathavan, D. Arivuoli, G. Attolini, C. Pelosi, Appl. Surf. Sci. 180 (2001) 119.
[2] D. Galusek, F.L. Riley, R. Riedel, J. Am. Ceram. Soc. 84 (2001) 1164.
[3] E. Martínez, J. Romero, A. Lousa, J. Esteve, Appl. Phys. A 77 (2003) 419.
[4] T.H. Fang, S.R. Jian, D.S. Chuu, Appl. Surf. Sci. 228 (2003) 365.
[5] S.R. Jian, T.H. Fang, D.S. Chuu, J. Electron. Mater. 32 (2003) 496.
[6] S.R. Jian, T.H. Fang, D.S. Chuu, J. Non-Cryst. Solids 333 (2004) 291.
[7] R. Pérez, M.C. Payne, A.D. Simpson, Phys. Rev. Lett. 75 (1995) 4748.
[8] G.S. Smith, E.B. Tadmor, N. Bernstein, E. Kaxiras, Acta Mater. 49 (2001) 4089.
[9] U. Landman, W.D. Luedtke, N.A. Burnham, R.J. Colton, Science 248 (1990) 454.
[10] J. Li, K.J.V. Vlient, T. Zhu, S. Yip, S. Suresh, Nature 418 (2002) 307.
[11] K.J.V. Vlient, J. Li, T. Zhu, S. Yip, S. Suresh, Phys. Rev. B 67 (2003) 104105.
[12] P. Walsh, R.K. Kalia, A. Nakano, P. Vashishta, S. Saini, Appl. Phys. Lett. 77 (2000) 4332.
[13] P. Walsh, A. Omeltchenko, R.K. Kalia, A. Nakano, P. Vashishta, S. Saini, Appl. Phys. Lett. 82 (2003) 118.
[14] T.F. Page, W.C. Oliver, C.J. McHargue, J. Mater. Res. 7 (1992) 450.
[15] J. Tersoff, Phys. Rev. B 39 (1989) 5566.
[16] M. Nakamura, H. Fujioka, K. Ono, M. Takeuchi, T. Mitsui, M. Oshima, J. Cryst. Growth 209 (2000) 232.
[17] J.M. Haile, Molecular Dynamics Simulation: Elementary Methods, Wiley, New York, 1992.
[18] T.H. Fang, C.I. Weng, J.G. Chang, Surf. Sci. 501 (2002) 138.
[19] Y.R. Jeng, P.C. Tsai, T.H. Fang, Nanotechnology 16 (2005) 1941.
[20] D. Hull, D.J. Bacon, Introduction to Dislocations, Butterworth-Heinemann, Oxford, 2001.
[21] J.E. Bradby, J.S. Williams, J. Wong-Leung, S.O. Kucheyev, M.V. Swain, P. Munroe, Phil. Mag. A 82 (2002) 1931.
[22] F. Giuliani, S.J. Lloyd, L.J. Vandeperre, W.J. Clegg, Inst. Phys. Conf. Ser. 179 (2003) 123.
[23] A.B. Mann, J.B. Pethica, Phil. Mag. A 79 (1999) 577.
[24] G. Patriarche, E. Le Bourhis, Phil. Mag. A 80 (2000) 2899.
[25] C.R. Taylor, E.A. Stach, G. Salamo, A.P. Malshe, Appl. Phys. Lett. 87 (2005) 073108.
[26] W.C. Olive, G.M. Pharr, J. Mater. Res. 7 (1992) 1564.
[27] K.L. Johnson, Contact Mechanics, Cambridge University Press, Cambridge, 1985.